Nanocatalysis

International Edition: DOI: 10.1002/anie.201701640
German Edition: DOI: 10.1002/ange.201701640

Dumbbell-Shaped Bi-component Mesoporous Janus Solid Nanoparticles for Biphasic Interface Catalysis

Tianyu Yang[+], Lijuan Wei[+], Lingyan Jing, Jifen Liang, Xiaoming Zhang, Min Tang, Michael J. Monteiro, Ying (Ian) Chen, Yong Wang, Sai Gu, Dongyuan Zhao, Hengquan Yang, Jian Liu,* and G. Q. Max Lu*

Abstract: *There is a strong desire to design and synthesize catalysts that assemble at the oil–water interface to improve the efficiency of biphasic reactions. Anisotropic dumbbell-shaped bi-component mesoporous carbon–organosilica Janus particles with asymmetric wettability are synthesized through a one-step compartmentalized growth of a mesoporous organosilica sphere attached to a mesoporous resorcinol–formaldehyde (RF) sphere. A library was prepared of tunable Janus particles possessing diverse hollow structures with various functionalities. As a proof of concept, the Janus particle-derived catalyst can assemble at the oil–water interface to stabilize Pickering emulsions. Owing to the increased reaction interface area, the Janus catalyst exhibits a more than three-fold increase in catalytic efficiency compared to the Pt loaded carbon sphere catalyst in aqueous hydrogenation reactions.*

Organic–aqueous biphasic catalysis reactions have long been used as an important platform for organic transformations, bio-refineries, and enzymatic reactions.[1] Despite extensive applications, these catalysis reactions still suffer from low reaction efficiency because of limited reaction interface areas.[1a,2] The solid particle-stabilized emulsion (so-called Pickering emulsion) is emerging as a promising solution to address this issue because solid particle emulsifiers are not only more separable than conventional molecular surfactants[3] but can also act as catalyst supports amenable to loading catalytic active sites. Notwithstanding intensive attempts, the reported interface-active catalysts are mainly limited to homogenous particles.[4] In contrast, Janus particles with asymmetric structures and wettability are desirable because the two sides can be positioned in their respective affinitive phase, that is, oil or water phase, leading to thermodynamically stable Pickering emulsions.[5]

It is well-recognized that the emulsifying abilities of Janus particles strongly depend on their morphology and chemical composition.[6] To date, sphere,[6d–f] rod,[6g] film,[6h] snowman,[6i] mushroom,[6j] and dumbbell[6k] Janus particles have been successfully synthesized. Among these morphologies, dumbbell-shaped Janus particles are an ideal candidate for designing interface-active solid catalysts because they are inclined to be in a single orientation perpendicular to the oil–water interface,[5b] thus allowing for exquisite controls over chemical reactions in biphasic mixtures reported by Resasco and coworkers.[1f] However, the existing dumbbell-shaped Janus particles are limited to polymers, while porous Janus inorganic particles are rare. Although several groups have synthesized Janus porous silica particles, these particles eventually grow to core–shell-like or snowman-like, rod-like structures owing to the extreme difficulty in tuning the interfacial energy during anisotropic growth.[7]

Herein, we present a facile wet-chemistry method to synthesize mesoporous carbon–organosilica Janus nanoparticles with a perfect dumbbell shape through a one-step growth of an organosilica sphere from a mesoporous resorcinol–formaldehyde (RF) sphere using dual surfactants to tune interfacial energy and porosity, as shown in Scheme 1. The as-prepared mesoporous RF spheres acting as the base nanoparticle are first synthesized by a dual soft-template route (F127 and FC4) as previously reported.[7d] The periodic mesoporous organosilica (PMO) particle is attached to the

[*] Dr. T. Yang,[+] L. Wei,[+] L. Jing, J. Liang, Dr. X. Zhang, Prof. H. Q. Yang
School of Chemistry and Chemical Engineering, Shanxi University
Taiyuan 030006 (PR China)
E-mail: hqyang@sxu.edu.cn
Dr. J. Liu
Department of Chemical Engineering, Curtin University
Perth, WA 6845 (Australia)
E-mail: jian.liu@curtin.edu.au
Dr. T. Yang,[+] Prof. M. J. Monteiro, Dr. J. Liu
Australian Institute for Bioengineering and Nanotechnology
The University of Queensland, Brisbane, QLD 4072 (Australia)
M. Tang, Prof. Y. Wang
Center of Electron Microscopy and State Key Laboratory of Silicon Materials, School of Materials Science and Engineering
Zhejiang University, Hangzhou 310027 (China)
Dr. T. Yang,[+] Prof. Y. I. Chen
Institute for Frontier Materials, Deakin University
Geelong, VIC 3216 (Australia)
Prof. D. Y. Zhao
Department of Chemical Engineering, Monash University
Clayton VIC 3800 (Australia)
and
Department of Chemistry and Laboratory of Advanced Materials
Fudan University, Shanghai 200433 (PR China)
Prof. S. Gu, Dr. J. Liu
Department of Chemical and Process Engineering
University of Surrey, Guildford, Surrey, GU2 7XH (UK)
Prof. G. Q. M. Lu
University of Surrey, Guildford, Surrey, GU2 7XH (UK)
[+] These authors contributed equally to this work.
Supporting information and the ORCID identification number(s) for the author(s) of this article can be found under: https://doi.org/10.1002/anie.201701640.

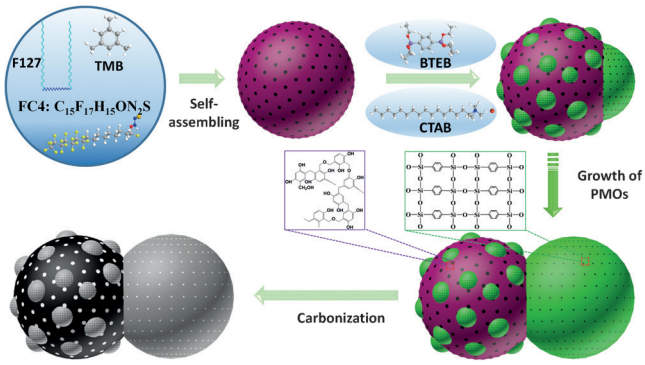

Scheme 1. Graphic illustration of the synthesis of the Janus nanoparticles.

RF sphere during hydrolysis and condensation of the organosilica precursor 1,4-bis(triethoxysilyl)benzene (BTEB) under alkaline condition aided by the dual surfactants FC4 and hexadecyltrimethylammonium bromide (CTAB). As a proof of concept, the Janus particle-derived catalysts are tested to be interface-active for forming Pickering emulsions and can efficiently promote biphasic hydrogenation reactions even without stir. Such Janus particles exemplify an innovative use in interface catalysis.

As the SEM image in Figure 1 A shows, the as-synthesized Janus nanoparticle consists of a smooth PMO compartment of 165 nm and a rough RF resin polymer compartment of 180 nm. The rough surface on the RF compartment results from multiple PMO nucleus deposited on the RF compartment surface. The TEM image (Figure 1 B) shows a clear mesoporous structure in the PMO and RF compartment, respectively; with a wormlike mesopores in the PMO part and an ordered mesopores in the RF part. The high-resolution TEM image (Figure 1 C) shows that the RF compartment has a mesoporous structure with pore size of 7 nm. Furthermore,

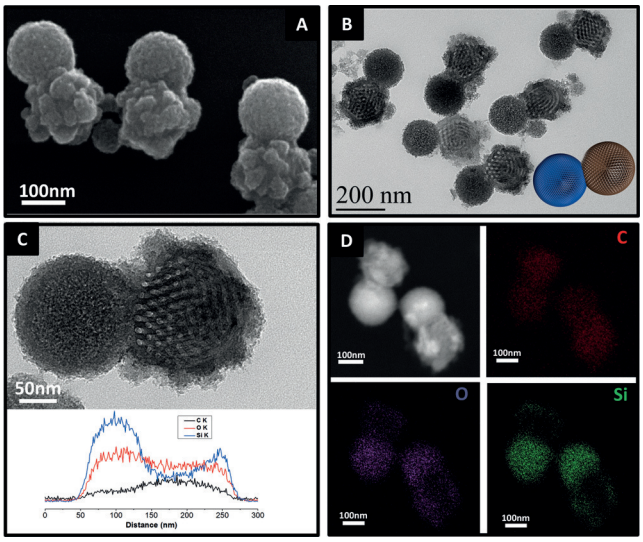

Figure 1. A) SEM image of as-prepared Janus RF&PMO nanoparticles. B) Low- and C) high-magnification TEM images of the as-synthesized Janus RF&PMO nanoparticles. D) HAADF-STEM image and corresponding EDS elemental mappings of as-synthesized RF&PMO nanoparticles.

the small PMO islands deposited on the RF compartment are about 30 nm in diameter. Its corresponding EDS line scan spectrum illustrates that the PMO compartment is rich in silicon; however, the RF compartment is carbon-rich. This is in agreement with the molecular structure of RF and PMO. The EDS mapping data in Figure 1 D further confirm the composition difference in the two compartments of the unique Janus structure. Moreover, the RF polymer compartment can be converted to mesoporous carbon spheres via carbonization under N_2, yielding C&PMO Janus particle (BET surface area: 541 $m^2 g^{-1}$), as shown in the Supporting Information, Figure S1. The C&PMO Janus particle exhibits excellent stability since there is no significant weight loss at temperatures below 550 °C (Supporting Information, Figure S2). Interestingly, the RF polymer compartment can also be selectively removed via calcination in air. As shown in the Supporting Information, Figure S1, the Janus silica nanoparticles have one side with a hollow cage structure after removal of the RF polymer. The hollow Janus silica nanoparticle increased the BET surface area up to 900 $m^2 g^{-1}$, compared to its Janus RF&PMO counterpart (BET surface area: 565 $m^2 g^{-1}$). To confirm the progeny role of FC4 surfactant, the RF&PMO Janus nanoparticles were synthesized in the absence of FC4. The TEM images in the Supporting Information, Figure S3 indicated the PMO compartment turned to a less porous structure with the same particle size by decreasing the amount of FC4. As shown in Figure S4, the resulting FC4-CTAB co-surfactant complex may provide higher interaction with organosilane BTEB to construct porous structure in the self-assembly process, which is also indicated in the solid NMR results (Supporting Information, Figure S5).

The asymmetric growth of the PMO compartment can be controlled by using the cationic surfactant CTAB. The morphological evolution of the Janus solid RF&PMO nanoparticles before hydrothermal treatment in different CTAB concentrations was studied. Without CTAB, the PMO layer uniformly coated the surface of the RF nanoparticle to form RF@PMO core–shell nanoparticles (Figure 2). In comparison, in the presence of CTAB, the PMO compartment grew asymmetrically on the surface opposite. CTAB concentration can also control the size of the PMO compartment. Increasing the CTAB concentration from 5.1 to 20.4 mM, the size of the PMO compartment increased from 127 to 157 nm (Figure 2). Therefore, the volume ratio of the two compartments of the Janus nanoparticles can be controlled from the RF dominated snowman to the dumbbell as confirmed by SEM images (Supporting Information, Figure S6).

Furthermore, the BTEB concentration can also control the PMO compartment size and the PMO shell thickness on the RF compartment. The TEM images in Figure 2 indicated that with the BTEB concentration increase from 5.0 to 31.5 μM, the size of PMO compartment increased from 70 to 125 nm and the PMO shell thickness in the RF compartment increased from 6 to 34 nm. We consider that at a high BTEB concentration, the BTEB-CTAB complex can form a larger cluster. Therefore, the resulting Janus nanoparticle at higher BTEB concentration not only had a larger PMO compartment but a thicker PMO shell.

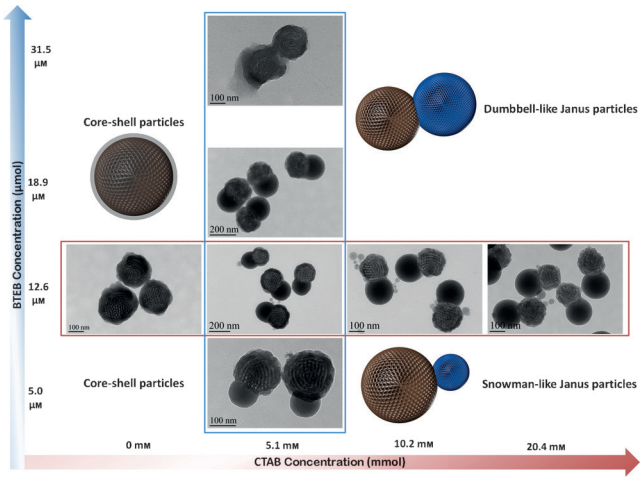

Figure 2. Illustration of the evolution and TEM images of Janus RF&PMO nanoparticles synthesized with different CTAB and BTEB concentrations.

The proposed formation mechanism is proposed below. First, the BTEB precursor consisting of the hydrophobic phenylene group interacted with the CTAB hydrophobic tail via hydrophobic interactions to generate small micelle clusters. Second, the new anionic surface on the clusters with hydroxy functional groups could be exposed during BTEB silane hydrolysis and condensation. Thereafter, the BTEB-CTAB complex with a cationic CTAB head attached and condensed on the surface of the new generated anionic surface via electrostatic interactions. The growth direction can be controlled by the sequence of CTAB addition as shown in the Supporting Information, Figure S7. The PMO compartment can keep growing asymmetrically with the assistance of CTAB. The asymmetric growth process can be rationalized by Equation (1):[7c,8]

$$\Delta G = \gamma_{1\text{-}2} + \gamma_{2\text{-}s} - \gamma_{1\text{-}s} \quad (1)$$

where ΔG refers to total Gibbs free energy change, $\gamma_{1\text{-}2}$ is the interfacial energy between RF and PMO, depending on the bonding strength and compaction of the crystal lattice near the junction of the two phase, $\gamma_{2\text{-}s}$ is the interfacial energy of PMO and the solvent, and $\gamma_{1\text{-}s}$ is the interfacial energy between RF and the solvent.

At the initial stage, once the BTEB-CTAB complex overcomes the nucleation energy barrier, it starts to nucleate at the interface of RF following a heterogeneous nucleation mechanism, and PMO nuclei appear at the interface of RF. As $\gamma_{2\text{-}s} < \gamma_{1\text{-}s}$ and the speed of hydrolysis and condensation is much faster than hetero-nucleation at the interface of RF, the growth of PMO at the interface of the as-formed embryos is much faster than the generation of new embryos at the interface of RF. Therefore, the growth mode of PMO prefers to take Volmer–Webber mode rather than Frank–van der Merwe mode,[7d] yielding Janus nanoparticles instead of core–shell structures. The key factor in forming a perfect dumbbell structure instead of the reported cubic-like or rod-like, core–shell-like structures may be due to the appropriate choice of mesoporous RF synthesized by FC4 and F127 dual surfactants, organosilane, surfactants, and solvent, allowing isotropic growth after the formation of embryos at the RF surfaces.

It is worth noting that Janus PMO can only be formed by using the organosilane with steric bridged group, as shown in the Supporting Information, Figure S8. To incorporate various organic groups (alkyl, aromatic, and heteroelement fragments) into this mesoporous Janus PMO compartment, this synthesis strategy can also be applied to form mesoporous Janus RF&PMO nanoparticle with multiple molecularly designed PMO compartments by adding different bridged organosilica precursors. According to the homology mechanism in organosilianes, we have doped multiple functional group including ethylene, ethane, thioether, and biphenyl functional groups (Supporting Information, Figure S9) into the original phenylene functional PMO framework to form dual functional PMO compartmented Janus nanoparticles. Organosilanes with organic ethylene, ethane, thioether, and biphenyl structures, respectively were co-hydrolyzed and co-condensed with BTEB to fabricate a phenylene plus dual-hybridized PMO Janus nanoparticle. Interestingly, the PMO compartment can transform to hollow structure via a controllable "multi-interface transformation" methodology with a void size of 70, 134 to 140 nm by incorporating thioether, ethane and ethylene fragment into the PMO compartment, respectively.

Our synthesis method allowed metal nanoparticles, for example Pt nanoparticles, to be selectively loaded on the RF compartment that was subsequently converted to carbon (see the Experimental Section in the Supporting Information), leading to a Janus catalyst Pt/C&PMO. As seen in Figure 3 A and the Supporting Information, Figure S10, monodispersed Pt nanoparticles with uniform particle size distribution (1–5 nm in size) were located selectively on the carbon compartment. As expected, this Janus catalyst can assemble at the oil–water interface, stabilizing a Pickering emulsion (Figur-

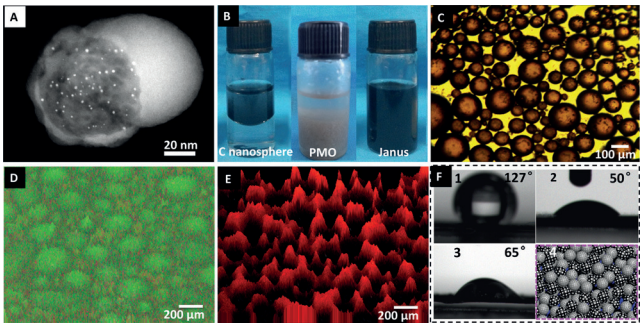

Figure 3. TEM image and interfacial assembly ability of the Janus catalyst Pt/C&PMO. A) HAADF-STEM image of a single Pt/C&PMO particle, B) appearance of the mixture of water and toluene in presence of C nanosphere, or PMOs, Pt/C&PMO particles (2 wt% with respect to water), C) optical micrograph of Pt/C&PMO-stabilized emulsion, D) 3D fluorescent optical micrograph of the Pt/C&PMO-stabilized emulsion with water phase dyed by FITC-dextran, E) 3D fluorescent optical micrograph of the Pt/C&PMO-stabilized emulsion with oil phase dyed by Nile Red, F) images of contact angle between a C nanosphere (1) or PMO (2), Pt/C&PMO (3) disk and a water droplet, and representation of the disk surface of Pt/C&PMO (4).

es 3B,C). The droplets, with sizes of 30–120 μm, are clearly observed with optical microscopy. Even after four weeks, the morphologies and sizes of droplets are well retained, indicating the high stability of this Pickering emulsion. Fluorescence-dye experiments confirmed that this Pickering emulsion was a water-in-oil type (Figures 3D,E) since the oil-soluble fluorescence dye and the water-soluble fluorescence dye are distributed in the continuous phase and the dispersed phase, respectively. In contrast, the pure carbon particles (derived from RF) and the PMO particles are both unable to stabilize Pickering emulsions since no droplets was observed (Supporting Information, Figure S11). This significant difference is due to their distinct surface wettability. As the results of the water contact angle measurement reveal (Figure 3F), the carbon is hydrophobic (127°) whereas PMO is hydrophilic (50°). Notably, the Janus particles exhibit a contact angle of 65°, which is between those of carbon nanosphere and PMO. This can be explained by the fact that in the sample disk used for contact angle measurements, some Janus particles stand with exposing hydrophobic carbon compartments to surface and others stand with exposing hydrophilic PMO compartments to surface (Figure 3F). As a result, Janus particles exhibit intervening wettability. These findings further confirm that the Janus particle indeed integrate two compartments with distinct wettability.

Subsequently, this Janus catalyst has been used for a typical biphasic reaction, Pt-catalyzed nitroarene reduction reaction. After vigorously stirring the biphasic reaction system in the presence of Pt/C&PMO (2000 rpm) numerous emulsion droplets appeared. After 6 h, nitrobenzene was fully converted to aniline under the stir-free conditions (Figure 4B). To check the role of the Janus structure, we prepared three counterpart catalysts, namely Pt/C (Pt loaded on carbon sphere), Pt/PMO (Pt loaded on PMO particle), and a dumbbell-shaped Janus catalyst (Pt/C&PMO double sides with Pt nanoparticles distributed on two sides) for comparison, as described in Figure 4A and their TEM images are shown in the Supporting Information, Figure S12. Under the identical conditions, Pt/C and Pt/PMO respectively gave conversions of only 15% and 8%, which are both much lower than that of the Pt/C&PMO catalyst. Such distinct comparisons confirm the role of Pt/C&PMO in boosting catalysis efficiency owing to the formation of Pickering emulsion. More interestingly, despite the same Janus structure, the reaction over Pt/C&PMO proceeded faster than Pt/C&PMO double sides. Remarkably, even under high stirring rate (900 rpm, at which the conversion no longer increased indicating elimilation of external diffusion), Pt/C offered a conversion of 89.6% (Supporting Information, Figure S13) within 6 h, which is still lower than that for the Janus catalyst under the stir-free conditions (>99%), futher delivering the merit of the Pt/C&PMO catalyst. Hydrogenation of other substrates including 2-nitrotoluene, 4-nitrotoluene, 2-nitroanisole, 4-nitroanisole, and 1-chloro-4-nitrobenzene further highlights the superiority of the Janus catalyst with 3–10 fold enhanced activity (Figure 4C). As shown in Figure 4D, $NaBH_4$ is confined within the water droplets and nitrobenzene confined in the interspaces between adjacent droplets owing to the droplet packing effects. As a result, the diffusion distances of

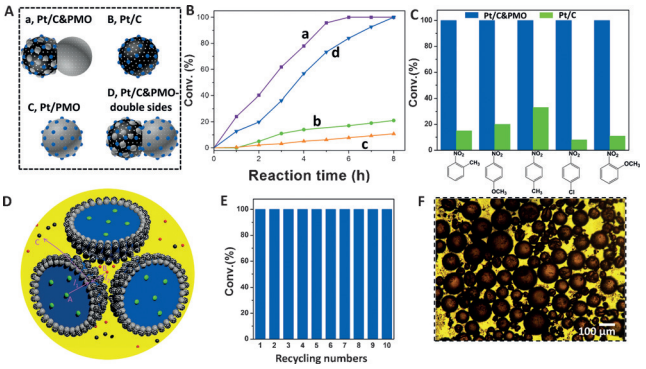

Figure 4. Results of nitroarene reductions (0.4 mL water, 1 mL toluene, 0.17 mmol nitroarene, 0.34 mmol $NaBH_4$ and 0.02 g Pt/C&PMO). A) Illustration of four catalysts including Pt/C&PMO, Pt/Carbon, Pt/PMO, and Pt/C&PMO double sides, B) the kinetic profile for nitrobenzene reductions over Pt/C&PMO, Pt/C, Pt/PMO, and Pt/C&PMO double sides under stir-free conditions, C) conversions of five different substrates in the catalysis reaction under stir-free conditions over Pt/C&PMO or Pt/C, and their reaction times corresponding to 7, 5, 5, 4, and 4 h, D) microscopic scenario of the reaction occurring in the Janus particle-stabilized emulsion, where A, B, and C represent $NaBH_4$, nitroarene, and aniline molecules, respectively, E) recyclability test of the Pt/C&PMO in the biphasic hydrogenation, reaction time: 6–7 h. F) Optical micrograph of the reaction system in the 10th reaction cycle.

these two molecules are significantly shortened.[4g,9] The combination of the short diffusion distances, large reaction interfacial area and controlled reaction location accounts for the high reaction efficiency of Pt/C&PMO under stir-free conditions.

As expected, the Janus particle catalyst can be facilely separated and recovered from the reaction system through a simple centrifugation operation, which is normally unattainable for the system using molecular surfactants. When used in the second reaction cycle, the recovered Janus catalyst offered a full conversion of nitrobenzene. From the third to the tenth reaction cycle, the nitrobenzene conversions could always reach nearly 100% (Figure 4E). Even after ten reaction cycles, the Pickering emulsion coud be obtained (Figure 4F), indicating the permernent interfacial activity of the Janus catalyst. Furthermore, the Pt leaching is negligible, which is supported by the filtration test (Supporting Information, Figure S14).

In conclusion, mesoporous carbon–organosilica Janus nanoparticles have been successfully synthesized through a wet chemical method. The dual templating mechanism was found to be crucial in obtaining a perfect dumbbell structure. The porous structure, compartment size and framework functionality of the dumbbell bi-component Janus particles can be rationally designed and tailored. Moreover, this new synthesis method allows for metal nanoparticles to be region-selectively positioned in one compartment of the dumbbell. The Pt-loaded Janus catalyst shows excellent interfacial activity for stabilizing Pickering emulsions, leading to significantly enhanced reaction efficiency in the biphasic nitroarene hydrogenation reaction even under the stir-free conditions. Moreover, we can envision that the dumbbell-shaped mesoporous Janus nanoparticles will provide an interesting plat-

form for other potential applications including drug delivery, nanomotors, and energy storages.[10]

Acknowledgements

This work is supported by the Natural Science Foundation of China (201573136 and U1510105), Program for New Century Excellent Talents in University (NECT-12-1030), and Program for Youth Sanjin Scholar. J. Liu gratefully acknowledges the support of UQ Foundation Research Excellence Award, J. Liu, Y.C. and D.Y.Z. gratefully acknowledge Australian Research Council (ARC) Discovery Project program. T.Y.Y. acknowledges the support of Deakin University CRGS award.

Conflict of interest

The authors declare no conflict of interest.

Keywords: hydrogenation · Janus particles · mesoporous materials · nanocatalysis · Pickering emulsions

How to cite: *Angew. Chem. Int. Ed.* **2017**, *56*, 8459–8463
Angew. Chem. **2017**, *129*, 8579–8583

[1] a) P. Tundo, A. Perosa, *Chem. Soc. Rev.* **2007**, *36*, 532–550; b) C. J. Li, L. Chen, *Chem. Soc. Rev.* **2006**, *35*, 68–82; c) S. Minakata, M. Komatsu, *Chem. Rev.* **2009**, *109*, 711–724; d) M. P. Ruiz, J. Faria, M. Shen, S. Drexler, T. Prasomsri, D. E. Resasco, *ChemSusChem* **2011**, *4*, 964–974; e) H. Yang, T. Zhou, W. Zhang, *Angew. Chem. Int. Ed.* **2013**, *52*, 7455–7459; *Angew. Chem.* **2013**, *125*, 7603–7607; f) J. Faria, M. P. Ruiz, D. E. Resasco, *Adv. Synth. Catal.* **2010**, *352*, 2359–2364.

[2] a) V. Stepankova, S. Bidmanova, T. Koudelakova, Z. Prokop, R. Chaloupkova, J. Damborsky, *ACS Catal.* **2013**, *3*, 2823–2836; b) K. Piradashvili, E. M. Alexandrino, F. R. Wurm, K. Landfester, *Chem. Rev.* **2016**, *116*, 2141–2169.

[3] a) L. Schoonen, J. C. M. van Hest, *Adv. Mater.* **2016**, *28*, 1109–1128; b) S. Crossley, J. Faria, M. Shen, D. E. Resasco, *Science* **2010**, *327*, 68–72; c) M. Pera-Titus, L. Leclercq, J. M. Clacens, F. De Campo, V. Nardello-Rataj, *Angew. Chem. Int. Ed.* **2015**, *54*, 2006–2021; *Angew. Chem.* **2015**, *127*, 2028–2044; d) Z. Zhu, H. Tan, J. Wang, S. Yu, K. Zhou, *Green Chem.* **2014**, *16*, 2636–2643; e) X. Yang, Y. Liang, Y. Cheng, W. Song, X. Wang, Z. Wang, J. Qiu, *Catal. Commun.* **2014**, *47*, 28–31.

[4] a) H. Yang, L. Fu, L. Wei, J. Liang, B. P. Binks, *J. Am. Chem. Soc.* **2015**, *137*, 1362–1371; b) L. Feng, J. Wang, L. Chen, M. Lu, Z. Zheng, R. Jing, H. Chen, X. Shen, *ChemCatChem* **2015**, *7*, 616–624; c) W. Zhou, L. Fang, Z. Fan, B. Albela, L. Bonneviot, F. De Campo, M. Pera-Titus, J. M. Clacens, *J. Am. Chem. Soc.* **2014**, *136*, 4869–4872; d) W. Zhang, L. Fu, H. Yang, *ChemSusChem* **2014**, *7*, 391–396; e) Z. Chen, H. Ji, C. Zhao, E. Ju, J. Ren, X. Qu, *Angew. Chem. Int. Ed.* **2015**, *54*, 4904–4908; *Angew. Chem.* **2015**, *127*, 4986–4990; f) J. Liu, G. Lan, J. Peng, Y. Li, C. Li, Q. Yang, *Chem. Commun.* **2013**, *49*, 9558–9560; g) C. Wu, S. Bai, M. B. Ansorge-Schumacher, D. Wang, *Adv. Mater.* **2011**, *23*, 5694–5699; h) D. C. Dewey, C. A. Strulson, D. N. Cacace, P. C. Bevilacqua, C. D. Keating, *Nat. Commun.* **2014**, *5*, 4670–4678; i) M. Dhiman, V. Polshettiwar, *J. Mater. Chem. A* **2016**, *4*, 12416–12424.

[5] a) F. Tu, D. Lee, *J. Am. Chem. Soc.* **2014**, *136*, 9999–10006; b) B. J. Park, D. Lee, *ACS Nano* **2012**, *6*, 782–790; c) B. P. Binks, P. D. I. Fletcher, *Langmuir* **2001**, *17*, 4708–4710; d) J. W. Kim, J. W. Cho, J. H. Cho, B. J. Park, Y.-J. Kim, K.-H. Choi, J. W. Kim, *Angew. Chem. Int. Ed.* **2016**, *55*, 4509–4513; *Angew. Chem.* **2016**, *128*, 4585–4589.

[6] a) J. Z. Du, R. K. O'Reilly, *Chem. Soc. Rev.* **2011**, *40*, 2402–2416; b) L. Carbone, P. D. Cozzoli, *Nano Today* **2010**, *5*, 449–493; c) G. Loget, A. Kuhn, *J. Mater. Chem.* **2012**, *22*, 15457–15474; d) S. Jiang, Q. Chen, M. Tripathy, E. Luijten, K. S. Schweizer, S. Granick, *Adv. Mater.* **2010**, *22*, 1060–1071; e) K.-H. Roh, D. C. Martin, J. Lahann, *Nat. Mater.* **2005**, *4*, 759–763; f) H. Ujiie, A. Shimojima, K. Kuroda, *Chem. Commun.* **2015**, *51*, 3211–3214; g) A. Kuijk, A. van Blaaderen, A. Imhof, *J. Am. Chem. Soc.* **2011**, *133*, 2346–2349; h) F. Liang, K. Shen, X. Qu, C. Zhang, Q. Wang, J. Li, J. Liu, Z. Yang, *Angew. Chem. Int. Ed.* **2011**, *50*, 2379–2382; *Angew. Chem.* **2011**, *123*, 2427–2430; i) H. Hu, F. Ji, Y. Xu, J. Yu, Q. Liu, L. Chen, Q. Chen, P. Wen, Y. Lifshitz, Y. Wang, Q. Zhang, S.-T. Lee, *ACS Nano* **2016**, *10*, 7323–73306; j) M. Feyen, C. Weidenthaler, F. Schüth, A.-H. Lu, *J. Am. Chem. Soc.* **2010**, *132*, 6791–6799; k) J. He, M. J. Hourwitz, Y. J. Liu, M. T. Perez, Z. H. Nie, *Chem. Commun.* **2011**, *47*, 12450–12452.

[7] a) X. Wang, B. Guan, Y. He, Y. Zhang, Y. Cao, Y. Liu, Z.-A. Qiao, Q. Huo, *ChemNanoMat* **2015**, *1*, 562–566; b) T. Suteewong, H. Sai, R. Hovden, D. Muller, M. S. Bradbury, S. M. G. U. Wiesner, *Science* **2013**, *340*, 337–341; c) X. Wang, Y. P. He, C. Liu, Y. L. Liu, Z.-A. Qiao, Q. Huo, *Nanoscale* **2016**, *8*, 13581–13588; d) X. M. Li, L. Zhou, Y. Wei, A. M. El-Toni, F. Zhang, D. Y. Zhao, *J. Am. Chem. Soc.* **2014**, *136*, 15086–15092; e) J. Liu, T. Yang, D.-W. Wang, G. Q. M. Lu, D. Y. Zhao, S. Z. Qiao, *Nat. Commun.* **2013**, *4*, 2798; f) T. Yang, R. Zhou, D.-W. Wang, S. Jiang, Y. Yamauchi, S. Qiao, M. J. Monteiro, J. Liu, *Chem. Commun.* **2015**, *51*, 2518–2521; g) J. Liu, N. P. Wickramaratne, S. Z. Qiao, M. Jaroniec, *Nat. Mater.* **2015**, *14*, 763–774; h) J. Croissant, X. Cattoen, M. W. C. Man, P. Dieudonne, C. Charnay, L. Raehm, J. O. Durand, *Adv. Mater.* **2015**, *27*, 145–149.

[8] S. G. Kwon, G. Krylova, P. J. Phillips, R. F. Klie, S. Chattopadhyay, T. Shibata, E. E. Bunel, Y. Liu, V. B. Prakapenka, B. Lee, E. V. Shevchenko, *Nat. Mater.* **2015**, *14*, 215–223.

[9] L. Wei, M. Zhang, X. Zhang, H. Xin, H. Yang, *ACS Sustainable Chem. Eng.* **2016**, *4*, 6838–6843.

[10] a) F. Wang, G. M. Pauletti, J. Wang, J. Zhang, R. C. Ewing, Y. Wang, D. Shi, *Adv. Mater.* **2013**, *25*, 3485–3489; b) X. Ma, K. Hahn, S. Sanchez, *J. Am. Chem. Soc.* **2015**, *137*, 4976–4979; c) S.-N. Yin, S. Yang, C.-F. Wang, S. Chen, *J. Am. Chem. Soc.* **2016**, *138*, 566–573; d) X. Wang, X. Feng, G. Ma, L. Yao, M. Ge, *Adv. Mater.* **2016**, *28*, 3131–3137; e) A. Walther, A. H. E. Müller, *Chem. Rev.* **2013**, *113*, 5194–5261; f) D. Yi, Q. Zhang, Y. Liu, J. Song, Y. Tang, F. Caruso, Y. Wang, *Angew. Chem. Int. Ed.* **2016**, *55*, 14733–14737; *Angew. Chem.* **2016**, *128*, 14953–14957.

Manuscript received: February 14, 2017
Revised manuscript received: March 20, 2017
Version of record online: May 4, 2017

